Original Research Paper

Vehicle emissions analysis for horizontal curves on two-lane rural highways – case study in Texas

Boya You[1], Fengxiang Qiao[1,*], Lei Yu[1], Junqing Shi[2]

[1] *Department of Transportation Studies, Texas Southern University, 3100 Cleburne Avenue, Houston, TX 77004*

[2] *College of Engineering, Zhejiang Normal University, Jinhua 321004, China*

Abstract

Vehicle emissions can seriously impact human daily life in a variety of ways and eventually has an impact on public health. It is believed that driving behavior is one of the most important factors impacting vehicle emissions. However, some other factors may also contribute to vehicle emissions indirectly, such as the geometric elements of a roadway. The objective of this paper is to explore the relationship between horizontal curve radii and vehicle emissions on two-lane rural highways through field tests under real-world driving conditions. The modeling results indicates that horizontal curves with a smaller curve radius tend to impose a higher workload on drivers and causes additional acceleration maneuvers. According to the exponential models, there are no large differences in the deceleration pattern between curvature and tangent when the curve radius is larger than 8,824 m, while the threshold for the acceleration pattern is 14,286 m. The results also indicate that aggregated data will better describe the relationship between vehicle

emissions and curve radius. Moreover, the results indicate that compared to driving on straight roads, a vehicle tends to generate less emissions when approaching the curve and generate more emissions when leaving the curve.

Keywords:

emission factor; roadway design; horizontal curve; driving behavior analysis

*Corresponding author. Tel: 713-313-1915, FAX 713/313-1856; Email: qiao_fg@tsu.edu (Fengxiang Qiao, PhD, Professor).

1 Introduction

The focus of air quality studies has traditionally been placed mainly on urban areas, but has been expanded to rural areas along with urban sprawl (FHWA, 2004). Air quality issues due to vehicle emissions can impact human daily life in a variety of ways. For example, nitrogen oxides (NOx) and hydrocarbon (HC) emissions from fuel combustion contribute to the formation of ozone, thus affecting daily life, industry, transportation, urbanization, and many other scenarios (EPA, 2016).

To estimate vehicle emissions, many mathematical models have been developed at macroscopic and microscopic levels (EPA, 2010; Frey *et al*, 2002; Claggett and Houk, 2008). The main focus has been placed on linkages with vehicle speed and acceleration rate because driving behavior has always been considered as the most important contributor to vehicle emissions (Claggett and Houk, 2008). With the increasing applications of connected and automated vehicles, however, computers are gradually taking more control from human drivers, which means that driving patterns will become more similar and easier to identify (Frey *et al*, 2007). Factors such as pavement roughness and roadway geometric elements will likely become more evident in emission estimation with the assumption that a majority of vehicles on the road are automated.

Horizontal curves, which are the segments that provide a gradual change in direction, are important elements in roadway design. Due to the difficulties in judging road condition, drivers may apply the brakes or tap the gas pedal to safely navigate winding segments, which can then generate extra curve-related vehicle emissions. According to the AASHTO Roadway Design Manual, also known as the Green Book, roadway alignment is selected first based on right-of-way consideration, which does not take vehicle emissions into account (Ward *et al*, 2003).

Most of macroscopic emission models are unable to properly estimate vehicle emissions because they neglect the special driving pattern on horizontal curves. For microscopic emission models, the challenge will be data availability because these models often require a series of inputs such as a speed file and acceleration rate (AASHTO, 2004). Therefore, it is important to explore and develop a feasible way for roadway designers to estimate vehicle emissions, especially for two-lane rural highways.

The motivation behind this study is to explore and develop a feasible way for roadway designers to

58 estimate vehicle emissions for horizontal curves on two-lane rural highways as vehicle emissions is not
59 currently taken into account in contemporary roadway design methods adopted by the FHWA. To
60 achieve this goal, there are three sub-objectives including developing an algorithm to gain geometric
61 data, developing models to quantify the relationship between curve radii and acceleration, and the
62 identification of the linkages between vehicle emissions and geometric features of horizontal curves.

63 **2 Literature highlights**

64 *2.1 Emission models and modeling techniques*

65 Many emission models have been developed at both macroscopic and microscopic levels to effectively
66 estimate vehicle emissions. The emission modeling tool MOVES developed by the EPA and EMFAC
67 developed by the California Air Resources Board estimate emissions through three steps: determining
68 a set of emission factors, generating vehicle activity, and estimating vehicle emissions by multiplying
69 results from the first two steps (EPA, 2010; AASHTO, 2004; Van Aerde and Rakha, 2009). One main
70 drawback of these macro level models is that the estimation may not sufficiently reflect real-world
71 emissions as they do not consider driving dynamics (Barth et al, 1996; NRC, 2000; Kelly and Groblicki,
72 1993).

73 Modal-emissions models have been developed in order to estimate vehicle emissions at a micro
74 level. According to Frey et al., there are basically two ways to develop modal-emission models (EPA,
75 2010): one is to develop a speed-acceleration matrix to classify the operating mode of vehicles (Kelly
76 and Groblicki, 1993), and another way is to develop the modal models based on engine mapping (West
77 et al, 1997). The Mobile Emission Assessment System (MEASURE) developed by the Georgia Institute
78 of Technology is able to estimate CO, NO_x, and VOCs using an aggregated modal modeling approach
79 (Shih ***et al***, 1997). Another modal model developed by Barth et al. predicts vehicle emissions for light-
80 duty vehicles based on a series of vehicle operating modes (Barth *et al*, 1996).

81 *2.2 Driver behavior on horizontal curves*

82 To identify the linkages between horizontal curves and vehicle emissions, it is important to understand

how drivers negotiate curves while driving. As shown in Fig. 1, a horizontal curve can be divided into four segments: approach, curve discovery, entry and negotiation, and exit (Fomunung *et al*, 2001). The driving tasks for a driver during curve discovery are to determine curvature, assess roadway conditions, make additional speed adjustments, and adjust path for curve entry (Fomunung *et al*, 2001). When approaching a horizontal curve, a driver makes judgments and adjusts vehicle speed before the Point of Curvature (PC), and then accelerates after passing the midpoint of the curve where driver has the highest visual demands to safely navigate a curve. A study conducted by the Virginia Tech Transportation Institute suggests that a driver starts decelerating around 50 to 100 ft before the PC and this distance is affected by demographic distribution (age, gender, driving experience) (Campbell, 2012). Another study examined the deceleration/acceleration pattern and concluded that deceleration ended close to the midpoint on small radius curves. For larger radius curves, deceleration ends right after PC and the start point of acceleration moves to the midpoint of curve (Machiani *et al*, 2016).

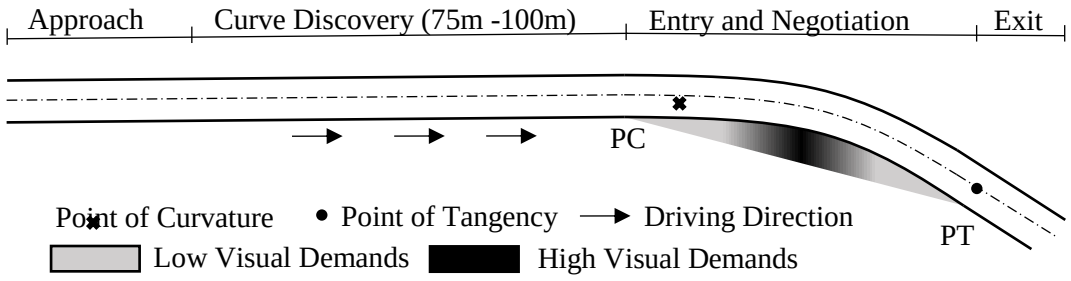

Fig. 1 Driving tasks on horizontal curvature

Several models have been developed in previous studies to estimate operating speeds using data collected from given spots (point of curvature, midpoint of curve, point of tangent, etc.). Currently, these models have been used to generate the speed file and to predict crash rates on horizontal curves. Nevertheless, few studies utilize these models to estimate vehicle emissions. A study conducted by Ko generated the speed file for horizontal curves using a speed prediction model and calculated vehicle emissions using the default database from MOVES (Ko, 2011).

2.3 Extraction of geometric information

In order to study the relationship between geometric features and vehicle emissions, one challenge is how to obtain geometric information about roadway alignment because of the difficulties in retrieving the original design files.

A GPS-based method has been applied in previous studies to collect data to compute curve radius and the results showed that GPS was able to accurately provide alignment data (Sanders, 2005; Imran and Patterson. 2006; Pratt *et al*, 2009). Pratt et al. used a GPS-based method to collect data every 25 feet to calculate the radius and recommended posted speeds for horizontal curves (Pratt *et al*, 2009). Sanders used a GPS/GIS method to extract geometric features for horizontal curves, where GPS was used to produce the centerlines of roadways and then the curve data were extracted through GIS (Sanders, 2005).

Many applications have been developed to identify geometric features for horizontal curves from digital maps. For example, Google Earth Pro developed by GOOGLE can be used to manually identify horizontal curves by fitting the curves with a radius-changeable circle (Google, 2016). Curve Extension developed for the Florida Department of Transportation, Curve Finder developed for the New Hampshire Department of Transportation, and Curve Calculator developed by ESRI are all GIS based curve-extraction tools. The Curve Extension and Curve Calculator can be used to identify some geometric elements for a single circular curve, while the Curve Finder can be used to extract several curves on a designated route at one time (Osei-Asamoah and Jackson, 2015). One major drawback of manually extracting geometric features from digital maps is that this neglects spiral transitions, which provide a gradual transition between tangents and circular curves. Another drawback of this method is the difficulty in determining the starting point of a curvature when the radius is large.

3 Methodology

3.1 Data preparation and pre-processing

First, data screening techniques were applied to remove outliers and some invalid records produced by test equipment due to vehicle vibration and connection problems. Outliers were identified based on commonsense knowledge (e.g. abnormal acceleration values) and three-sigma rule. Then latitude and

longitude was converted into Gauss-Kruger x-y coordinates. Subsequently, the Rolling Algorithm was developed in the next step to calculate the curve radius. Additionally, all the data pairs were re-arranged according to their geo-locations through interpolation.

3.2 Rolling algorithm

The Rolling Algorithm (RA) was developed and applied in this study to calculate curve radius. As shown in Fig. 2 (a), a radius-changeable circle rolls through the data set ordered by geolocation at a rolling speed of 1 point/time. When this circle stops at point *i* (Fig. 2 (b)), the coordinates of point *i*, point *i*-1 and point *i*+1 are read and used to identify the perpendicular bisectors of point *i*-1 and point *i*, point *i* and point i+1. The coordinates of the center point can be calculated by solving equation (1), (2), and (3). Lastly, the curve radius can be calculated by measuring the distance between the center point and point *i*. Compared to the method of manually extracting geometric features from digital maps, the RA can identify both the radius of simple curves and also spiral curves. It should be noted that the lower the speed, the higher the accuracy of this algorithm. For example, if the speed of a test vehicle is 80 km/h, which equals to 22.22 m/s, the distance between two consecutive points will be approximately 22 m. The curve length needs to be at least 44 m ($22\,\mathrm{m} \times 2 = 44\,\mathrm{m}$) to ensure the accuracy of the calculated radius at one point on each curve. A curve length that is longer than 88 m ($22\,\mathrm{m} \times 4 = 88\,\mathrm{m}$) is favorable, and ensures the accuracy of the calculated radius at three points.

$$A\begin{bmatrix} x_{ii} \\ y_{ii} \end{bmatrix} = b \tag{1}$$

$$A = \begin{bmatrix} (x_i - x_{i-1})/(y_i - y_{i-1}) & 1 \\ (x_{i+1} - x_i)/(y_{i+1} - y_i) & 1 \end{bmatrix} \tag{2}$$

$$b = \begin{bmatrix} (y_{i-1} + y_i)/2 + (x_i - x_{i-1}) * (x_{i-1} + x_i)/(2 * y_i - 2 * y_{i-1}) \\ (y_i + y_{i+1})/2 + (x_{i+1} - x_i) * (x_i + x_{i+1})/(2 * y_{i+1} - 2 * y_i) \end{bmatrix} \tag{3}$$

Where x_{ii} and y_{ii} are the coordinates of center point, x_i and y_i are the coordinates of point *i*, x_{i-1} and y_{i-1} are the coordinates of point *i-1*, x_{i+1} and y_{i+1} are the coordinates of point *i+1* showing in Fig. 2 (b).

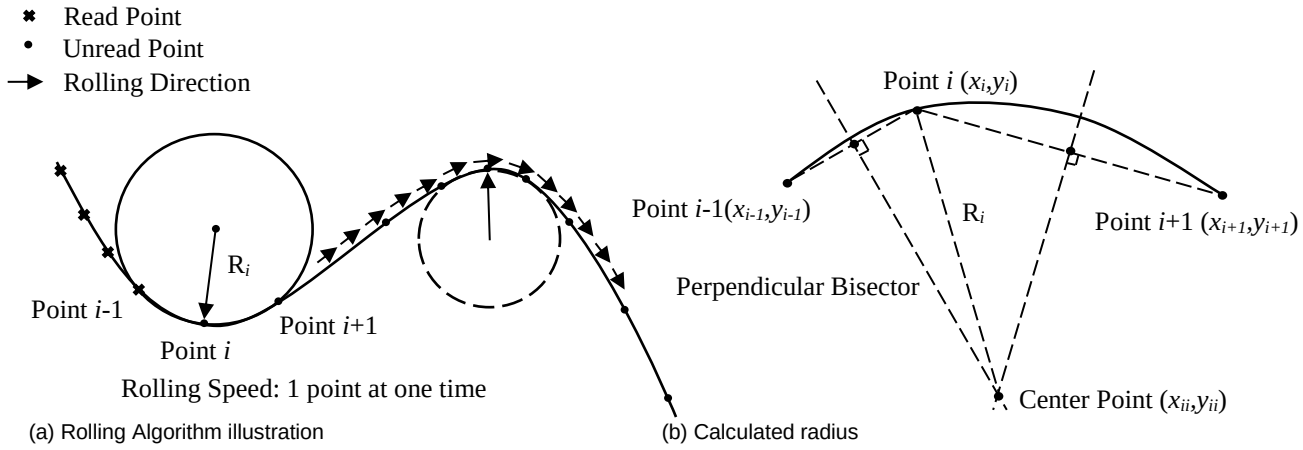

(a) Rolling Algorithm illustration (b) Calculated radius

Fig. 2 Rolling algorithm overview.

3.3 Moves operating mode distribution

The purpose of MOVES operating mode distribution analysis is to provide an overview of activity data distribution, which could help to better understand the driving pattern on horizontal curves. First, vehicle specific power (VSP) was calculated based on instantaneous speed, and acceleration/deceleration. The equation for VSP calculation is (Nam, E. K, 2003):

$$VSP = v * 1.1 * a + (9.81 * grade(\%) + 0.132) * v + 0.000302 * v^3 \quad (4)$$

Where *v* is the instantaneous vehicle speed in the unit of m/s, *a* is the second-by-second acceleration in the unit of m/s^2. The grade is the roadway longitudinal grade, which was determined by field measurement or from the roadway profile. After generating the VSP, the data for each second was assigned to a specific operating mode bin as defined in MOVES.

3.4 Critical events

To further study the relationship between horizontal curve radius and acceleration/deceleration, the data

set was split into groups depending on curve radius (150 m – 450 m, 450 m – 750 m…). The number of critical events was counted under each group. Critical events in this study are defined based on two types of driving maneuvers: braking and accelerating. A data point that qualifies with the following criteria was considered as a critical event in this study:

Critical event A (accelerating): if the acceleration of i^{th} second is larger than or equal to, or the accelerations of $(i\text{-}2)^{th}$, $(i\text{-}1)^{th}$, and i^{th} second are all larger than or equal to , i^{th} second is considered as a critical event A.

Critical event B (braking): if the acceleration of i^{th} second is less than or equal to, or the accelerations of $(i\text{-}2)^{th}$, $(i\text{-}1)^{th}$, and i^{th} second are all less than or equal to , i^{th} second is considered as a critical event B.

Considering the uneven distribution of data points, the proportion of critical events (PCE) has been used as an analysis index instead of the number of critical events. PCE is calculated by dividing the number of critical events in group *i* by the sample size of group *i* as shown in equation (5).

$$PCE = \frac{Number\ of\ critical\ events\ in\ group\ i}{Sample\ size\ of\ group\ i} \quad (5)$$

Two exponential models were developed to estimate the proportion of critical events on different curve radius. In the meantime, groups with small sample sizes were removed from the analysis to ensure the confidence level (95%). See equation (6):

$$Proportion\ of\ critical\ event_{A/B} = \beta_1 e^{\beta_2 \cdot Curve\ radius} \quad (6)$$

3.5 Curvature conversion factor

The average emission factors of tangents on two-lane rural highways were calculated in this study as baselines. As shown in equation (7), the emission factors of a curvature were calculated as a product of the emission factor of tangents (EF) and Curvature Conversion Factor (CCF).

$$Emission\ Factor_{entry/exit} = Curvature\ Conversion\ Factor(CCF) \times Emission\ Factor_{tangent} \quad (7)$$

4 Field Test

4.1 Site selection

Most previous studies related to geometric design, especially for horizontal curves, focuses on two-lane rural highways. This is because two-lane rural highways have relatively lower traffic volume and fewer signalized intersections. Further, these roads have a variety of geometric features. Therefore, this paper focuses on two-lane rural highways in order to provide more robust field-testing data.

Considered that vehicle speed would be affected by the amount of traffic on the road and the number of intersections, to rule out the impact of other vehicles on road, the overall data collection process was done in a free flow condition. The horizontal curve radius is the only geometric feature considered in this study. A series of criteria for site choice were defined as below: (1) two-lane rural highway; (2) a variety of geometric characteristics (curve radius, curve type); (3) constant geometric elements (lane width, shoulder width, etc.); (4) same posted speed limit (50 mph $\approx$ 80 kph); (5) constant pavement type; and (6) data availability.

4.2 Test plan

The Scenic Loop in Livingston, TX was selected as the test site for this study (Fig. 3). The test vehicle was a 2009 Honda C-RV and the fuel type was gasoline. The length of the test route was 9.66 kilometers (6 miles). The driver was required to drive 10 rounds on the test route under free flow conditions from the same direction to keep the vehicle in a similar lane position.

Fig. 3 Test route.

4.3 Test Equipment

A Portable Emission Measurement Systems (PEMS) was used in this study for data collection, which provides second-by-second data records including longitude, latitude, instantaneous vehicle speed, acceleration/deceleration, and emission data.

5 Results and discussion

5.1 Driving behaviors on horizontal curve

The impact of a horizontal curve on driving activities was studied to identify the linkages between horizontal curve and vehicle emissions because vehicle emissions are highly related to vehicle speed and acceleration.

Scatter Plots of Activity Data

The calculated curve radius generated by RA varies from 150 m to infinity, which represents the 'radius' of tangents. As shown in Fig. 4 (a), 'low-speed' data points are concentrated between 150 m and 500 m, which represent a small-radius range. When the curve radius increases to a certain level, speed samples oscillate around 80 km/h, which is the posted speed limit. Drivers scan the curve for information and slow down when approaching the curve, and then accelerate to resume normal speed when they

feel comfortable with the driving workload imposed by the curves. In addition to the speed-radius scatter plot, MOVES operating mode bins were used to analyze the distribution of activity data. Fig. 4 (b) shows the MOVES mode bin distribution along an x-axis, which represents the curve radius. The majority of data points fall in the radius range of 0 m and 7,000 m. Bin 0, which is defined as braking, only exists in a radius range of 0 m to 5000 m. There was no data point that matched Bin 1, which represents idling. Most data points fall in a middle- and high-speed range (Bin 21 – Bin 40).

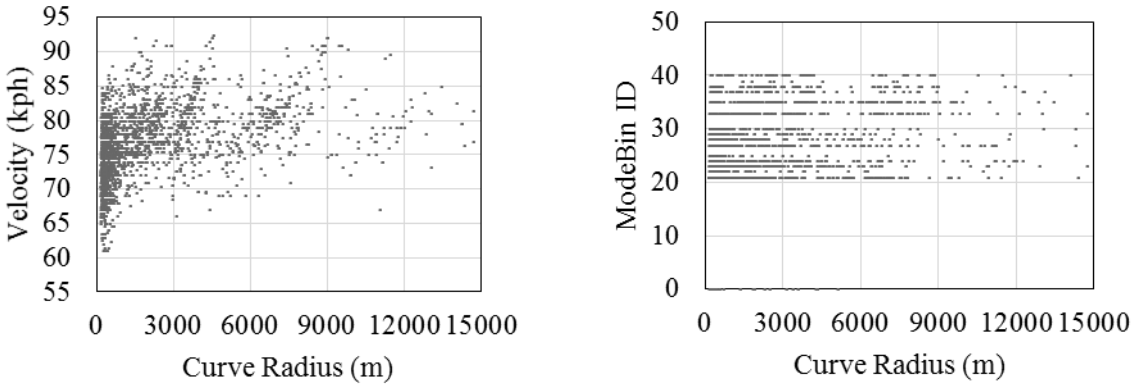

(a) Scatter plot of velocity and curve radius (b) MOVES operating mode bin distribution

Fig. 4 Scatter plots of activity data.

The scatter plots present an overview of the relationship between activity data and curve radius, which helps to better understand the data distribution. However, vehicle emissions tend to be larger when burning more fuel. Therefore, in addition to this analysis, critical events have been defined to analyze the acceleration maneuver.

Analysis of Critical Events

Fig. 5 shows the relationship between the number of critical events and curve radius. The majority of the number of critical event A (Fig. 5 (a)) and critical event B (Fig. 5 (b)) concentrate in a radius range of 150 m to 4,000 m, which means that a driver tends to accelerate and decelerate more frequently on curvature with a smaller curve radius. Very few critical events exist when the curve radius is larger than 4,000 m. From these two graphs, a threshold of 4,000 m has been determined as curvature-to-tangent

boundaries, which means a point where the curve radius is larger than 4,000m is considered as belonging to a tangent. Considering the data distribution, PCE values were calculated and are presented in Fig. 5 (c) and Fig. 5 (d). The normalization results indicate that a smaller curve radius tends to generate more critical events.

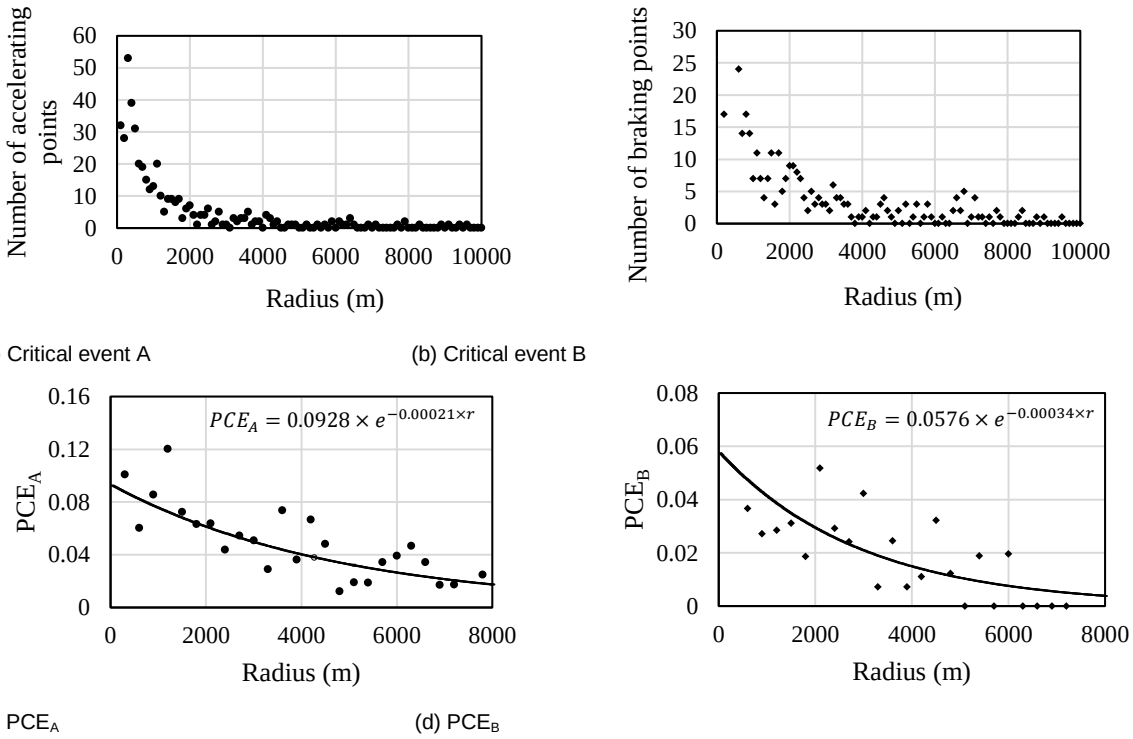

(a) Critical event A (b) Critical event B

(c) PCE_A (d) PCE_B

Fig. 5 Number of critical events.

To better understand the downtrend in the number of critical events, two exponential models were developed to calibrate the PCE value. Seventy percent of the data points were used for calibration, while 30% of the data points were used for validation. The calibration results of PCE_A and PCE_B are shown in equation (9) and equation (10). The small *p*-value of the coefficients of intercept (*p*-value$_{interceptA} = 6.11 \times 10^{-13} < 0.05$, *p*-value$_{interceptB} = 7.45 \times 10^{-9} < 0.05$) and curve radius (*p*-value$_{radiusA} = 1.48 \times 10^{-5} < 0.05$, *p*-value$_{radiusB} = 0.014 < 0.05$) means that these two factors have a significant impact on PCE value. The validation root mean square error (RMSE) of equation (9) is 11.5%, while that of equation (10) is 9.4%.

Black thick lines in Fig. 5 (c) and Fig. 5 (d) represent the predicted results from these two exponential models. The yield point of these fitting lines can be identified through these equations. Take PCE_B as an example, the yield point of the fitting line is 8,824 (8,824 = (1/0.00034)×3, where (1/0.00034) is a time constant in Equation (10), the times 3 means the termination of termination periods of an exponential curve like the one in Fig. 5 (d)). This means that when the curve radius is larger than 8,824 m, there are no large differences between PCE_B for curves with a larger radius. Similarly, the threshold of PCE_A is 14,286 m. Compared to accelerating, the braking on a curvature is more sensitive to curve radius (the threshold of 8,824 m is smaller than 14,286 m). When curve radius increases, the number of critical event B decreases faster than the number of critical event A.

$$PCE_A = 0.0928 \times e^{-0.00021 \times curve\ radius} \quad (9)$$

$$PCE_B = 0.0576 \times e^{-0.00034 \times curve\ radius} \quad (10)$$

Driving Behaviors on Four Curve Types

Fig. 6 illustrates different driving patterns affected by four curve types found from data analysis. On a simple curve or a spiral curve, driving behavior follows a similar pattern: a driver will decelerate before entering the curve and then accelerate after they pass the midpoint of a curve. On a reverse curve or a compound curve, if the tangent between two curvatures is long enough then this allowed drivers to adjust vehicle speed to a normal level. The driving behaviors on reverse curves and compound curves are similar to simple curves. As such, a reverse curve or a compound curve could be divided into two single curves. However, if the tangent between the curves is not long enough, there will be a 'shift.' It should be noted that even though the distribution of acceleration/deceleration points might be affected by curve types, drivers will need to accelerate and decelerate at least once for each single curve.

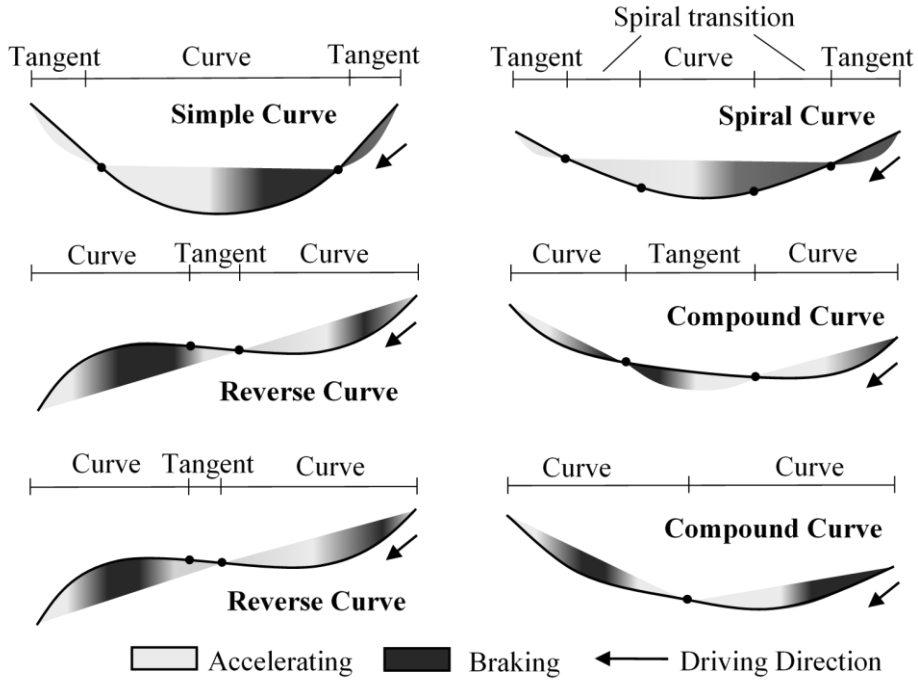

Fig. 6 Driving activity of different curve types.

This finding suggests that the linkages between acceleration data and curve radius are highly associated with geolocation. Take the spiral curve as an example (Fig. 6), the color transition from red to green indicates that a driver starts to accelerate at the midpoint of the curve where the curve radius is the smallest. As shown in Fig. 7, strong acceleration happens after the midpoint where the curve radius is larger (r_{amax}). The acceleration pattern will be significantly affected by factors including roadway condition and demographic distribution. For example, for commuters who are more familiar with the route, the acceleration tends to happen earlier. This finding also suggests that modeling with instantaneous data might not be a good way to explore the relationship between vehicle emissions and curve radius due to shifts in the acceleration pattern. As such, data aggregation might be a better approach.

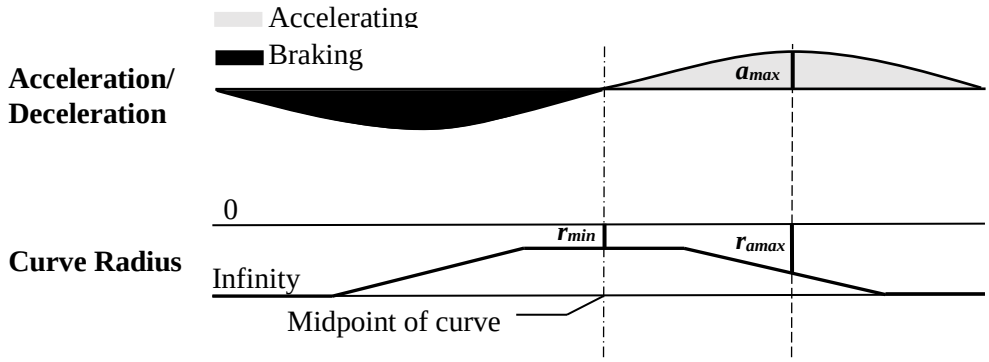

Fig. 7 Acceleration and curve radius.

5.2 Horizontal curve and vehicle emission

Bubble Chart for Acceleration and Vehicle Emissions

In this section, previous findings are further associated with vehicle emissions. The bubble charts below represent accelerations, calculated curve radius, and vehicle emissions associated with geolocation. The larger the absolute value, the larger the bubble size. As discussed in the methodology, longitude and latitude were converted into Gauss-Kruger x-y coordinates. The vertical and horizontal axis represent the x-y coordinates of data points. Fig. 8 (a) represents the accelerations on a reverse curve. Black bubbles represent deceleration, while green bubbles represent acceleration. The data collected from field testing was consistent with the analysis in the previous section. The reverse curve can be divided into two single curves for analysis. A similar approach can be applied to the compound curve shown in Fig. 8 (b). CO_2, CO and HC were positively related to acceleration. Compared to braking, accelerating tends to generate more emissions. More NO_x is generated at a deceleration/acceleration change point because more air is drawn in.

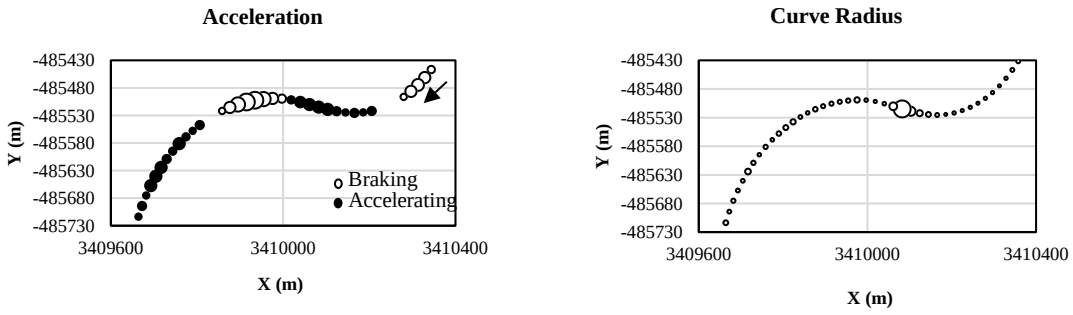

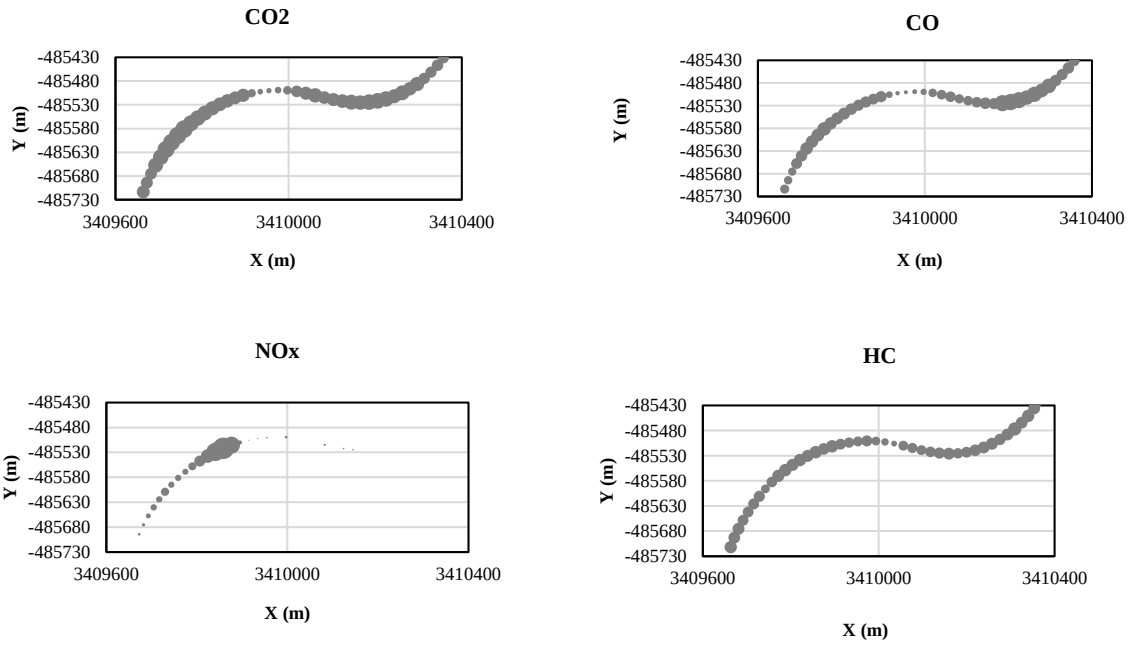

320

321

322 (a) Vehicle emissions on a reverse curve

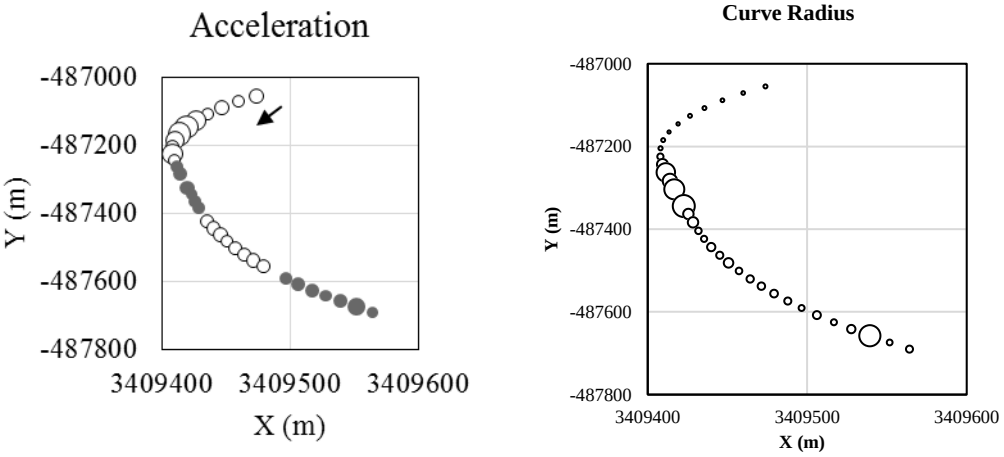

323

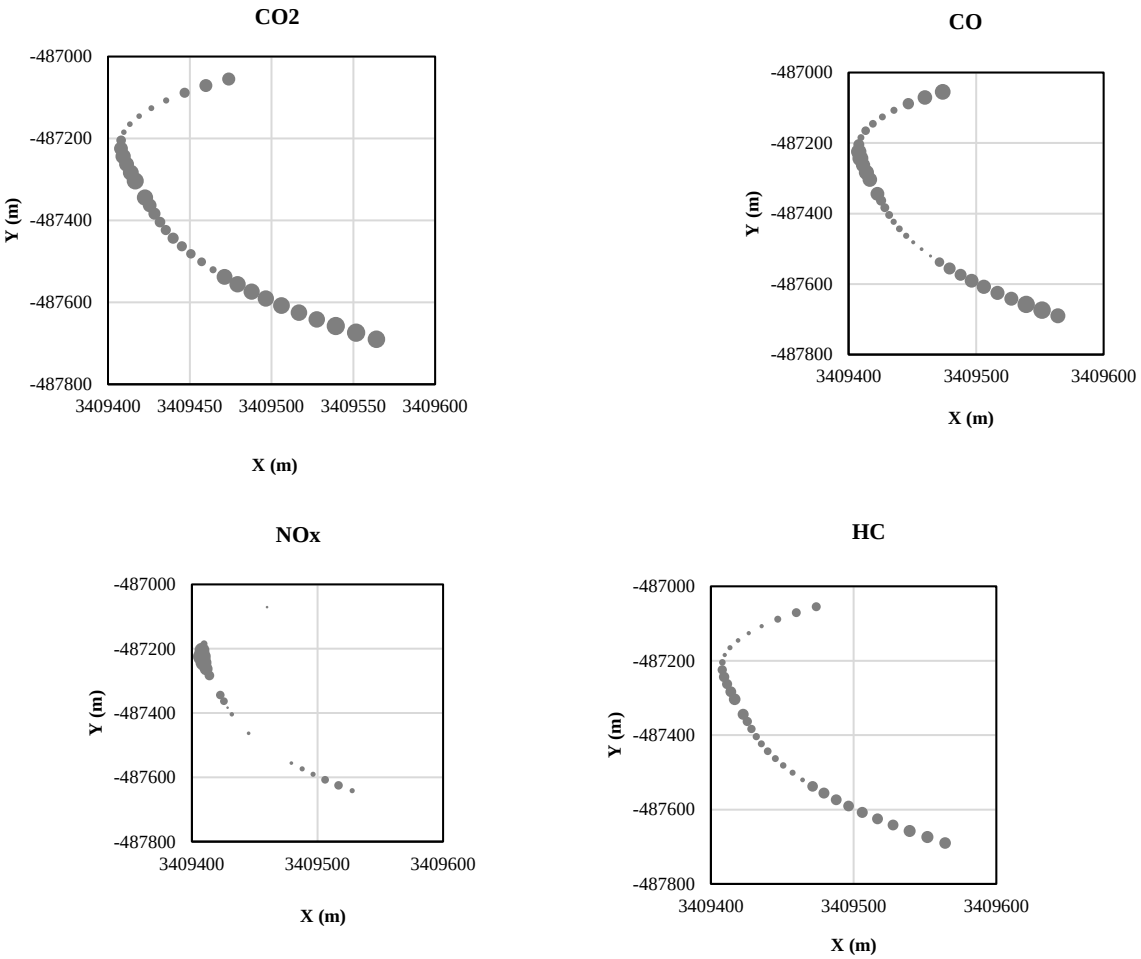

(b) Vehicle emissions on a compound curve

Fig. 8 Vehicle emissions varied by geo-location.

Similar to the acceleration pattern on curves shown in Fig. 7, the largest vehicle emissions are generated somewhere ahead of the midpoint of a curve. This finding suggests that the relationship between vehicle emissions and curve radius will also be affected by geolocation.

Emission estimation for horizontal curves

The CCF table was developed for highway design using interpolated emission data. Emission factors of tangents were viewed as baselines, which were normalized to 1 in this table. On average, the entry CDR is smaller than 1, which means that when approaching a curve, the vehicle tends to generate fewer emissions compared to driving on a straight road. Conversely, exit CDR is larger than 1, which means

that when leaving a curve, a vehicle accelerates and starts to resume normal speed, and therefore generates more emissions compared to driving on tangents. The length of entry and exit segments were also studied. As shown in the last column in Table 1, the length of entry was approximately twice the length of exit for different radius ranges.

Table 1 Curvature Discount Rate of Emission Factor

Factors	**CO**	**CO_2**	**HC**	**NO_X**	**Distance Factor**
Radius	Min. Radius – 500 m				
Entry CDR	0.706	0.717	0.773	0.983	2.02
Exit CDR	0.991	1.225	1.210	0.774	1.00
Radius	500 m – 1000 m				
Entry CDR	0.469	0.679	0.648	1.771	1.95
Exit CDR	1.098	1.307	1.184	0.964	1.00
Radius	1000 m – 5000 m				
Entry CDR	0.926	0.597	0.538	1.367	2.24
Exit CDR	0.852	1.337	1.158	0.866	1.00
Radius	∞				
Tangent CDR	1	1	1	1	N.A
$EF_{Tangent}$ (mg/m)	0.305	3040	0.779	0.054	N.A

Fig. 9 shows one example of CCF application. Assume that the designed radius of this simple curve is smaller than 500 m. This simple curve can be divided into two parts: entry segment and exit segment. The curvature discount rate of entry for a CO_2 segment is 0.72, while the curvature discount rate of an exit segment is 1.23. The emission factor of this horizontal curve is calculated as the product of curvature discount rate and emission factor of tangents. The length of entry and exit segments can be estimated using Distance Factor and the length of curve discovery as defined by NHTSA. Total emissions can be calculated as the product of emission factor and distance.

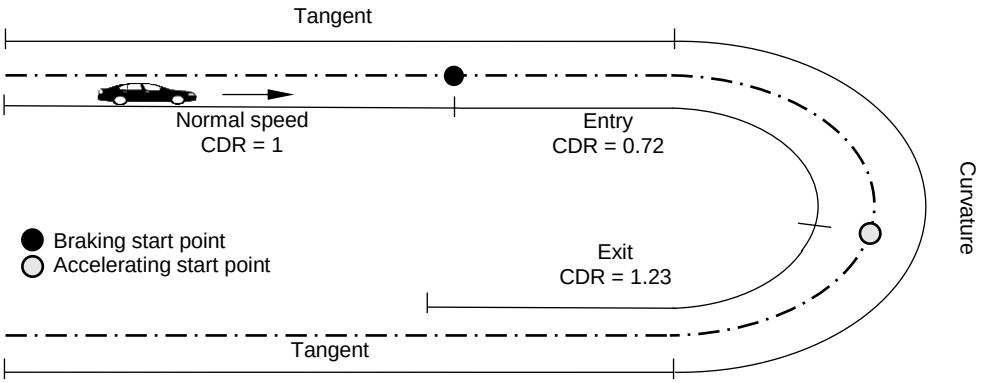

Fig. 9 Emission estimation using CCF.

6 Conclusions

The main outputs of this study include an algorithm to calculate the curve radius using GPS data, two exponential models to estimate critical events using curve radius, and an emission factor table to help roadway designers estimate vehicle emissions for horizontal curves.

The modeling results for this critical event indicates that horizontal curves with a smaller curve radius tend to impose a higher workload on drivers and causes additional acceleration maneuvers. According to the exponential models, there are no large differences in the deceleration pattern between curvature and tangent when the curve radius is larger than 8,824 m, while the threshold for the acceleration pattern is 14,286 m. This means that in the roadway design process, when the curve radius is larger than 8,824 m, designers do not need to adjust the emission factor for the entry segment of a curve using CCF. Similarly, emission factors applied to tangents can be directly used for curve emission estimation when the curve radius is larger than 14,286 m.

The results also indicate that aggregated data will better describe the relationship between vehicle emissions and curve radius because emission data is highly related to driving behavior, while curve features are associated with geolocation. The value of the Curvature Conversion Factor indicates that compared to driving on straight roads, a vehicle tends to generate less emissions when approaching the curve and generate more emissions when leaving the curve. Lastly, the Curvature Conversion Factor table categorizing curve radius into four groups was developed using real-world emission data,

and provides an easy and straightforward way for roadway designers to estimate emissions on horizontal curves.

7 Transferability and limitation

Transferability of the results is most relevant to the test procedures. Models and tables presented in this paper can be applied to similar cases, for example, to estimate vehicle emissions on two-lane rural highways under a free flow condition. This study utilized a light-duty vehicle for data collection, which is a factor that should be adjusted when calculating emissions for other vehicle types.

There are three main assumptions for the Curvature Conversion Factor table: one is that all the curves are assumed to be single curves, which means that a reverse curve or compound curve will need to be divided into two single curves for the calculation; the other two assumptions are that superelevation and roadway grade are assumed to be 0 due to the difficulty in collecting such data without the original drawing files or field measurements.

Acknowledgement

The authors acknowledge funding for this research is supported in part by the Tier 1 University Transportation Center TranLIVE #DTRT12GUTC17/KLK900-SB-003, and the National Science Foundation (NSF) under grant #1137732. The authors also wish to thank Mahreen Nabi who assisted in the data collection process. The opinions, findings, and conclusions or recommendations expressed in this material are those of the author(s) and do not necessarily reflect the views of the funding agencies.

References

Barth, M., F. An, J. Norbeck, and M. Ross. 1996. Modal emissions modeling: A physical approach. *Transportation Research Record: Journal of the Transportation Research Board*, (1520), pp. 81-88.

Book, G. 2004. *A policy on geometric design of highways and streets*. AASHTO, 5th Edition, pp. 1-56051.

399 Campbell, J.L. 2012. *Human factors guidelines for road systems* (Vol. 600). Transportation
400 Research Board.
401 Claggett, M. and Houk, J., 2008. Comparing MOBILE6. 2 and Emfac2007 emission factors.
402 *Transportation Research Record*: *Journal of the Transportation Research Board*, (2058),
403 pp.51-57.
404 EPA, U. 2010. *Motor Vehicle Emission Simulator (MOVES) User Guide.* US Environmental
405 Protection Agency.
406 EPA, U. Air Emission Sources. 2016. https://www3.epa.gov/air/emissions/basic.htm. Accessed
407 July 31, 2016.
408 Federal Highway Administration (FHWA). 2004. *Sample Methodologies for Regional Emissions*
409 *Analysis in Small Urban and Rural Areas*. U.S. Department of Transportation.
410 Fomunung, I., S. Washington, R. Guensler, and W. Bachman. 2001. Validation of the MEASURE
411 automobile emissions model: a statistical analysis. *Journal of Transportation and*
412 *Statistics*, pp.65-84.
413 Frey, H.C., Unal, A. and Chen, J., 2002. *Recommended strategy for on-board emission data*
414 *analysis and collection for the new generation model.* Prepared for Office of
415 Transportation and Air Quality, US Environmental Protection Agency.
416 Frey, H.C., W. J. Rasdorf, S. Pang, K. Kim, S. Abolhasani, and P. Lewis. 2007. Methodology
417 for activity, fuel use, and emissions data collection and analysis for nonroad construction
418 equipment. In *Proc., 100th Annual Meeting of the Air and Waste Management Association.*
419 Google Earth Pro. *Earth Help – Measuring Tool Features and Options.* Website –
420 https://support.google.com/earth/answer/148135?hl=en, Accessed July 30, 2016.
421 Imran, M., Y. Hassan, and D. Patterson. 2006. GPS–GIS-Based Procedure for Tracking Vehicle
422 Path on Horizontal Alignments. *Computer-Aided Civil and Infrastructure Engineering*.
423 21(5): 383-94.
424 Kelly, N.A. and P. J. Groblicki. 1993. Real-world emissions from a modern production vehicle
425 driven in Los Angeles. *Air & Waste*, 43(10), pp. 1351-1357.
426 Ko, M.H. 2011. *Incorporating vehicle emission models into the highway design process*.

427 Doctoral dissertation, Texas A&M University.
428 Machiani, S.G., A. Medina., R. Gibbons., and B. Williams. 2016. Driver Behavior Modeling on
429 Horizontal Curves for Two-Lane Rural Roads Using Naturalistic Driving Data.
430 In *Transportation Research Board 95th Annual Meeting.*
431 Montella, A. and L. L. Imbriani. 2015. Safety performance functions incorporating design
432 consistency variables. *Accident Analysis & Prevention*,74, pp.133-144.
433 Nam, E.K., 2003. Proof of concept investigation for the physical emission rate estimator (PERE)
434 for MOVES. EPA document, (420).
435 NRC. 2000. *Modeling Mobile-Source Emissions,* National Academy Press, National Research
436 Council. Washington, D.C.
437 Osei-Asamoah, A. and E. Jackson. 2015. Automated Horizontal Curve Classification and
438 Parameter Calculation Methods Using Vehicle-Collected Road Inventory Data.
439 In *Transportation Research Board 94th Annual Meeting* (No. 15-4700).
440 Pratt, M., J. D. Miles, and J. A. Bonneson. 2009. Workshops on Using the GPS Method to
441 Determine Curve Advisory Speeds. Texas Transportation Institute. Texas A&M University
442 System. Report No. FHW A/TX-10/5-5439-01-1.
443 Sanders, B. 2005. Updating Horizontal Curve Data Using GPS Centerlines. Kentucky
444 Transportation Cabinet. Division of Planning. Presentation at *the FHWA Highway*
445 *Performance Monitoring System (HPMS) Data Collection Workshop*. Salt Lake City, Utah.
446 Shih, R., Fable, S. and R.F. Sawyer. 1997. Effects of Driving Behavior on Automotive Emissions.
447 In *Seventh CRC On-Road Vehicle Emissions Workshop, San Diego, CA.*
448 Van Aerde, M. and H. Rakha. 2007. *INTEGRATION© Release 2.30 for Windows: User's Guide–*
449 *Volume I: Fundamental Model Features*. M. Van Aerde & Assoc., Ltd., Blacksburg.
450 Ward, D., I. Ibarra, and A. Ruddle. 2003. Threat analysis and risk assessment in automotive
451 cyber security. *SAE International Journal of Passenger Cars-Electronic and Electrical*
452 *Systems*, 6(2013-01-1415), pp. 507-513.
453 West, B.H., R. N. McGill, J. W. Hodgson, C. S. Sluder, and D. E. Smith. 1997. *Development of*
454 *data-based light-duty modal emissions and fuel consumption models*, No. 972910. SAE